

Alma Mater Studiorum Università di Bologna  
Archivio istituzionale della ricerca

Self-assembling of fibers inside an injectable calcium phosphate bone cement: a feasibility study

This is the final peer-reviewed author's accepted manuscript (postprint) of the following publication:

*Published Version:*

Di Filippo M.F., Giuri D., Marchiori G., Maglio M., Pagani S., Fini M., et al. (2022). Self-assembling of fibers inside an injectable calcium phosphate bone cement: a feasibility study. MATERIALS TODAY CHEMISTRY, 24, 100991-101004 [10.1016/j.mtchem.2022.100991].

*Availability:*

This version is available at: <https://hdl.handle.net/11585/902547> since: 2022-11-14

*Published:*

DOI: <http://doi.org/10.1016/j.mtchem.2022.100991>

*Terms of use:*

Some rights reserved. The terms and conditions for the reuse of this version of the manuscript are specified in the publishing policy. For all terms of use and more information see the publisher's website.

This item was downloaded from IRIS Università di Bologna (<https://cris.unibo.it/>).  
When citing, please refer to the published version.

(Article begins on next page)

This is the final peer-reviewed accepted manuscript of:

**[M.F. Di Filippo, D. Giuri, G. Marchiori, M. Maglio, S. Pagani, M. Fini, C. Tomasini, S. Panzavolta,**

**Self-assembling of fibers inside an injectable calcium phosphate bone cement: a feasibility study,**

**Materials Today Chemistry, Volume 24, 2022, 100991,]**

The final published version is available online at:  
**[\[https://doi.org/10.1016/j.mtchem.2022.100991\]](https://doi.org/10.1016/j.mtchem.2022.100991)**

Terms of use:

Some rights reserved. The terms and conditions for the reuse of this version of the manuscript are specified in the publishing policy. For all terms of use and more information see the publisher's website.

*This item was downloaded from IRIS Università di Bologna (<https://cris.unibo.it/>)*

***When citing, please refer to the published version.***

# Self-assembling of fibres inside an injectable calcium phosphate bone cement: a feasibility study

Maria Francesca Di Filippo<sup>1§</sup>, Demetra Giuri<sup>1§</sup>, Gregorio Marchiori<sup>2</sup>, Melania Maglio<sup>2</sup>, Stefania Pagani<sup>2</sup>, Milena Fini<sup>2</sup>, Claudia Tomasini<sup>1</sup>, Silvia Panzavolta<sup>1,3\*</sup>

<sup>1</sup>Department of Chemistry “G. Ciamician” University of Bologna via Selmi 2, 40126 Bologna, Italy

<sup>2</sup>IRCCS Istituto Ortopedico Rizzoli, Complex Structure of Surgical Sciences and Technology, via di Barbiano 1/10, 40136 Bologna, Italy

<sup>3</sup>Health Sciences and Technologies – Interdepartmental Center for Industrial Research (HST-ICIR), Alma Mater Studiorum - Università di Bologna, 40064 Ozzano dell’Emilia, Bologna, Italy.

§ these Authors equally contributed to this work

\* corresponding author:

Prof.ssa Silvia Panzavolta,

<sup>1</sup>Department of Chemistry “G. Ciamician” University of Bologna via Selmi 2, 40126 Bologna, Italy  
[silvia.panzavolta@unibo.it](mailto:silvia.panzavolta@unibo.it); +39 051 2099566

## Abstract

Calcium phosphate cements (CPCs) are biocompatible, bioactive and osteogenic systems which have the potential to mimic the mineral phase of native bone and the ability to be molded into bone defects and implant sites, then harden *in situ* to provide stability. However, their mechanical strength needs to be improved: in the last few decades, the incorporation of preformed fibres into a brittle cement matrix has been proven to increase the mechanical properties. To obtain a better cohesion between the fibres and the cement paste thus improving the mechanical performances, in this work we attempted the formation of self-assembling fibres in a single step during the setting of our calcium phosphate cement formulations.

The formation of fibres was achieved by introducing a low-molecular-weight gelator (MW< 1000 Da) derived from L-Dopa: Boc-L-Dopa(Bn)<sub>2</sub>-OH. This molecule can form supramolecular structures, owing to weak interactions, and chelate Ca<sup>2+</sup> ions to arrange into a fibrous network. The

morphological analysis revealed that the gel was able to form fibres even inside such a dense matrix and their presence provided mechanical reinforcement both when tested in compression and in bending. Micro-CT analyses showed no variation in the total porosity, but an increase of pores diameter was observed when fibres are present. Moreover, the reinforced cements were able to ensure good cell viability and to express the main gene markers that are necessary for bone formation.

**Keywords: Self-assembled fibres; mechanical reinforcement; Calcium phosphate bone cements; Low molecular weight gelator; biocompatibility**

## **Introduction**

The development of Calcium Phosphate Cements (CPCs) by Chow and Brown took place in the early 1980s<sup>1</sup>. CPCs are biocompatible and bioactive materials but their use in orthopedic surgery is limited due to their mechanical properties: in fact, they are brittle and have poor strength and toughness, if compared to those of native bone. These characteristics limit the use of CPCs to applications such as the treatment of maxillofacial defects, repair of craniofacial defects and dentistry<sup>2,3</sup>. An improvement in mechanical properties would considerably broaden the field of potential applications of calcium phosphates cements. This goal could be achieved for example through the preparation of composite materials. Among all the approaches for the preparation of composite cements, the use of fibres reinforcement is one of the most successful: in fact, it has been extensively explored even in the field of hydraulic cements and concretes for civil engineering and building applications<sup>4</sup>. Natural fibres (such as cellulose, sisal, jute, bamboo, asbestos, rock-wool, etc.)<sup>5</sup> and man-made fibres (such as steel, titanium, glass, carbon, polymers, etc.) have been proposed<sup>6</sup>, but, as far as found in literature, they have always been introduced inside the pasty material after their synthesis, with mixed results.

The main reasons for the failure of CPC-fibers reinforced lie in the low strength of the fibers, their insufficient length/diameter ratio and the poor adhesion between the fibers and the cement matrix: in fact, fibers of insufficient length are not able to transfer the load and may act as flaws in the material <sup>7</sup>. For a strengthening effect to occur, substantial load has to be transferred from the matrix to the fiber via the interface: crack initiation normally occurs with the matrix phase, whereas crack propagation is impeded or hindered by the fibers <sup>8</sup>. In fact, a prerequisite for an effective reinforcement relies on the mechanical properties of all the components and on the fiber-matrix adhesion, which is crucial for a successful load transfer. Unreinforced cements are characterized by a brittle behavior and an immediate fracture in two or more pieces, while in the case of fibre-reinforced CPCs (FRCPCs) a large amount of energy is absorbed during the fracture and the stress at break is higher <sup>7</sup>. The possibility to achieve a composite material reinforced with fibres grown directly inside the cement would represent a unique opportunity to obtain a better cohesion between fibres and cement paste. So far, no studies have reported the development of FRCPCs using fibres which were directly self-assembled inside bone cements.

In this work, the self-assembling of fibres was achieved using a low-molecular-weight gelator (LMWG) derived from commercial L-Dopa. LMWGs are molecules with a molecular weight lower than 1000 Da and a specific stereochemistry, that can self-assemble into supramolecular structures, such as gels and fibres. Unlike the conventional polymeric hydrogels that are mainly based on covalently crosslinked networks of polymers, the networks formed by these supramolecular hydrogels are due to noncovalent interactions including hydrogen bonds,  $\pi$ - $\pi$  stacking and Van der Waals force <sup>9</sup>. A LMWG may initiate the self-assembly process or phase transition by a stimulus or a triggering force (e.g., temperature, pH, or inorganic salt <sup>10</sup>), necessary to bias thermodynamic equilibrium: the gelator molecules self-assemble in long structures which entangle together, forming a network able to trap the solvent.

In a previous study, some of the authors found that Boc-L-Dopa(Bn)<sub>2</sub>-OH is a robust gelator able to self-assemble using calcium ions as trigger <sup>11-14</sup>. In particular, in presence of calcium and carbonate ions, the gelation process occurred during the formation of an inorganic crystalline phase, CaCO<sub>3</sub> crystals. The fibrous network of the gelator preserved its morphology even after the mineralization process, entrapping the crystals and penetrating inside them to create a composite organic/inorganic hybrid material, able to exchange calcium ions with the environment increasing its mechanical properties <sup>15</sup>. The ability to self-assemble into fibres in presence of calcium ions makes this gelator the perfect candidate to introduce inside CPCs.

LMWGs are biocompatible and able to form hydrogels under several conditions. Because of the striking resemblance between hydrogels and soft tissues, supramolecular hydrogels are used in the biomedical field for three-dimensional cell cultures, drug delivery purposes, antimicrobial applications, tissue engineering and regeneration of neural, cardiac, skin, cartilage and bone tissue <sup>16,17</sup>.

The main hurdle for the fibres growth in a cement matrix is the amount of liquid required for the formation of the networks. In fact, while hydrogels are mainly composed of a liquid phase (up to 99%), CPCs are made up of an inorganic powder mix that is necessary for the formation of the cement. The aim of this work was to demonstrate the feasibility to obtain self-assembling of fibres made of LMWG in CPCs thus improving mechanical properties and biocompatibility. Addition of Barium sulphate as radiopacifying agent was also evaluated <sup>18</sup>.

## **2. Materials and Methods**

### **2.1. Synthesis of Boc-L-Dopa(OBn)<sub>2</sub>-OH**

The gelator was synthesized from unprotected and commercially available L-Dopa, which was transformed into Boc-L-Dopa(Bn)<sub>2</sub>-OH following a multistep procedure in solution, as reported in literature<sup>19,20</sup>.

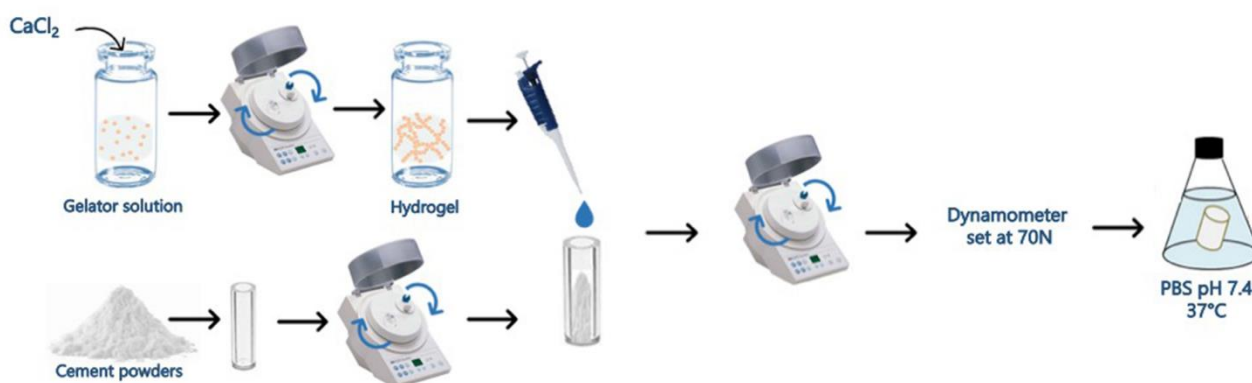
### 2.1.1 Preparation of the gelator solutions

The gelator solutions were prepared by dissolving the proper amount (20 and 50 mg, respectively) of Boc-L-Dopa(Bn)<sub>2</sub>-OH in 1 mL of an aqueous NaOH solution (1.3 equivalents), under stirring and sonicating for about 15 min<sup>10</sup>.

### 2.2. Cement preparation

The cement powders are composed of a gelatin/ $\alpha$ -TCP mix (15% w of gelatin with respect to the total amount) and CaHPO<sub>4</sub>·2H<sub>2</sub>O (DCPD), following a procedure previously reported<sup>21–23</sup>.

To obtain the reference cement (C), gelatin/ $\alpha$ -TCP powders and DCPD (5% w/w) were mixed in an electric mortar (3M ESPE RotoMix) two times for 20 s. After addition of an aqueous NaOH solution (1.3 equivalents) the powders were mixed again for 20 s with a liquid to powder (L/P) ratio = 0.52 mL/g. The obtained pastes were compacted in a Teflon mold for 1 min with a 4465 Instron dynamometer set at 70 N. Then, cements were demolded and put in phosphate buffer (PB) at 37°C and pH 7.4 for 7 days.



Scheme 1. Preparation method of the FRCPC.

For the preparation of fibres-containing cements, to ensure a homogeneous dispersion of the fibres inside the paste, different methods have been tested [See S.I.], showing that the formation of fibres does not depend exclusively on the concentration of the gelator solution and the amount of trigger, but it is also affected by the order they are mixed. The optimized preparation method is shown in Scheme 1. 1.3 equivalents (with respect to the weighted amount of the gelator) of  $\text{CaCl}_2$  as trigger were added to the gelator solution and mixed for 20 s in the electric mortar. Then, the cement powders were added to the obtained hydrogel (liquid to powder ratio of 0.52 mL/g) and treated as described above. Since increasing fiber content improves strength and fracture toughness <sup>8</sup>, two different amounts of gelator, 1% and 2.6% (w/w) with respect to the cement powders, were tested. The obtained cements were labeled G1 and G2.6, respectively. For the Ba-containing formulations, 10% (w/total weight of the cement powders) of  $\text{BaSO}_4$  was added to the cement powders before mixing with the liquid phase. The Ba-containing samples were labeled adding “\_Ba” to the above stated tags. The compositions and labels of the obtained cements are summarized in Table 1.

Table 1. Compositions and labels of the obtained CPC samples.

Label	$\text{CaCl}_2$ (1.3eq)	$\text{BaSO}_4$ (10% w/w)*	Gelator % (w/w)*
C	x		
C_Ba	x	x	
G1	x		1%
G1_Ba	x	x	1%
G2.6	x		2.6%
G2.6_Ba	x	x	2.6%

\* w/w with respect to the weight of the powders mix.

## 2.3. Cement characterization

### 2.3.1. Morphological analyses



Morphological investigation of the fractured surfaces of the cement samples was performed after stopping the hardening reaction with liquid nitrogen, using a Cambridge Stereoscan 360 Scanning Electron Microscope (SEM) with an electron acceleration voltage of 15kV. Samples were sputter-coated with gold prior to examination.

### **2.3.2. Measurement of fibre diameters**

The mean values of the fibre diameters were calculated from the SEM images using the Digimizer Image Analysis Software. At least 50 fibres were measured for each composition.

### **2.3.3. Structural Characterization**

For X-Ray diffraction analysis, the cements were extracted from PB and immediately immersed in liquid nitrogen. Samples were ground in a mortar, packed into recessed silicon slides and subjected to X-ray diffraction analysis by means of a Philips X'Celerator powder diffractometer equipped with a graphite monochromator in the diffracted beam. CuK $\alpha$  radiation was used (40 mA, 40 kV). The spectra were obtained in the 5–50 °/2 $\theta$  range using a 0.067° step and a 3°/min speed.

Fourier-transform infrared spectroscopy (FTIR, Nicolet IS10 spectrophotometer) was performed with a spectral resolution of 4 cm<sup>-1</sup> and 70 scans from 4000 to 500 cm<sup>-1</sup> on samples prepared as KBr disks. Omnic software (Thermo Electron Corp., Woburn, MA) was used for data processing and baseline correction.

### **2.3.4 Mechanical properties**

Mechanical characterization of the cements was performed both in compression and in bending mode on samples right after the extraction from PB. The compressive strength tests were performed using cylinder-shaped samples (6 mm in diameter and 12 mm high) submitted to increasing compression load at a crosshead speed of 1 mm/min by means of a 4465 Instron testing machine, equipped with a 1 kN load cell. At least ten specimens were tested for each formulation.

The specimens employed in the flexural tests were flat rectangular bars (20 x 10 x 3.5 mm) tested in three-point bending using a 4465 Instron testing machine, equipped with a 1 kN load cell at a crosshead speed of 1 mm/min. The flexural strength, Young's flexural modulus and work-of-fracture (WOF) were then measured from the load–displacement curves as described in equations 1, 2 and 3, respectively.

$$\text{Flexural Strength (MPa)} = \frac{3 \cdot F \cdot L}{2 \cdot b \cdot h^2} \quad 1)$$

where F is the failure load, L is the distance between outer loading points (20 mm), b and d are the width and the thickness of the specimen, respectively <sup>24</sup>.

$$\text{Flexural Modulus (MPa)} = \frac{F \cdot L^3}{4 \cdot d \cdot b \cdot h^3} \quad 2)$$

where d is the deflection at mid-span <sup>25</sup>.

$$\text{Work of Fracture (WOF)} = \frac{A}{b \cdot h} \quad 3)$$

where A indicates the total area under the load-displacement curve.

## 2.4 Rheological tests

The rheological analyses were carried out to evaluate the viscoelastic behavior of the Boc-L-Dopa (Bn)<sub>2</sub>-OH hydrogels in terms of G' (storage modulus, elastic contribution) and G'' (loss modulus, viscous contribution) moduli. The Anton Paar modular compact rheometer MCR102 was used for these tests. Time sweep tests were carried out on the gel keeping the shear strain (shear strain,  $\gamma$  = 0.5%) and the oscillation frequency (10 rad/s) constant, recording a point every 60 seconds for several hours.

## 2.5 Injectability and cohesion tests

The injectability of the obtained cements was evaluated as reported in a previous paper <sup>18</sup>. Cement powders (5 grams) were manually mixed in a mortar (the liquid to powder ratio was kept = 0.52

mL/g) and then transferred into a luer-lock 10 mL syringe fitted with an orifice of 1,2 mm inner diameter and a 14-gauge needle, specifically designed for injectability tests as reported in literature

<sup>26</sup>. Then, the syringe was placed between the compression plates of a 4465 Instron dynamometer equipped with a 1kN load cell, and the CPC paste was extruded from the syringe at a speed of 15 mm/min. Tests were performed at room temperature and each measurement was carried out in triplicate recording injectability curves. To assess the cements cohesion, pastes were extruded directly in PB solution, stored at 37°C and monitored at different times.

## 2.6. Micro-CT Characterization

C, C\_Ba, G1, G1\_Ba, G2.6 and G2.6\_Ba materials were scanned in the SkyScan 1172 micro-CT system (Bruker- MicroCT, Belgium) at a nominal resolution of 5 microns (2096x4000 pixels) employing a 0.5 mm thick aluminum filter and an applied x-ray tube voltage of 70 kV. Camera pixel binning was not applied. The scan orbit was 180 degrees with a rotation step of 0.4 degrees. Reconstruction was carried out using the SkyScanTMNRecon software (version 1.7.4.6, Bruker). Gaussian smoothing, ring artifact reduction and beam hardening correction were applied during the reconstruction process, and specific alignment relative to each single scan when needed. Volume of interest (VOI) selection, segmentation to binary and morphometric analysis were performed using SkyScan CT-Analyser ("CTAn" 1.20.3.0 version, Bruker) software. VOIs were defined considering the most structurally homogeneous region of the samples, starting from the center, and measuring a volume of at least  $75\% \pm 5$  of the total volume of each sample (Figure 1).

Then, the following 3D parameters related to the material porosity were calculated:

- the total porosity (%), defined as the ratio between the volume of the pores detected in the scaffolds and the total volume (VOI);
- the normalized frequency of the pore's distribution in the VOI

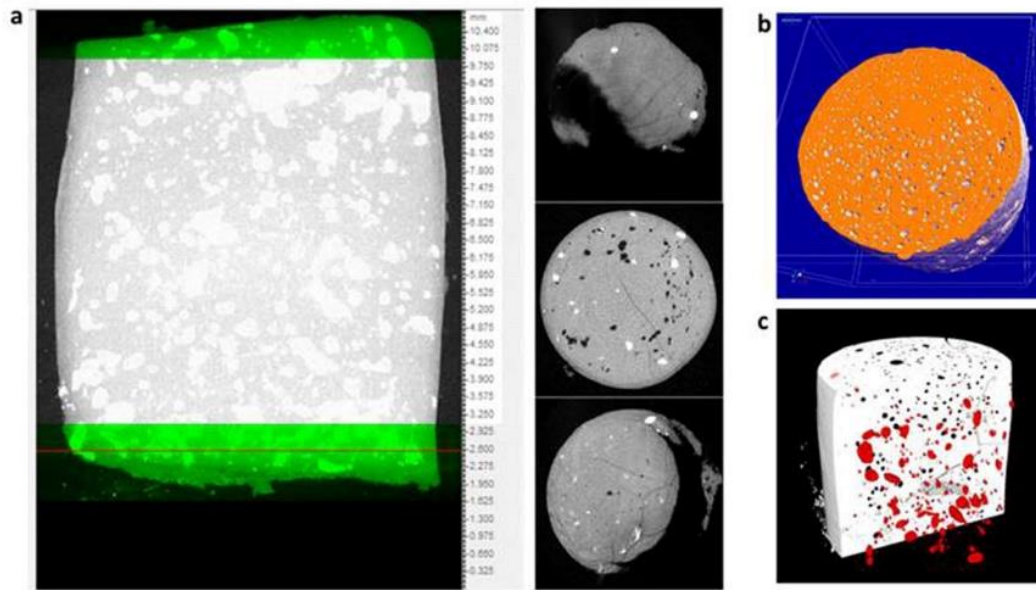


Figure 1. a) Definition of the VOI for the analyses. On the sagittal view, VOI top and bottom excluding incomplete sections (green regions); b) 3D visualization of G1 sample and c) 3D visualization of G1\_Ba sample, highlighting pores (in black) and barium particles (in red)

## 2.7 *In vitro* biocompatibility

*In vitro* biocompatibility was assessed on G1 and G2.6 cements, added or not with barium (G1\_Ba, G2.6\_Ba), using the sample without the gelator as reference (C\_Ba). After powder mixing with the liquid phase (Scheme 1), the obtained cylindrical samples were cut into slices (diameter = 6 mm, height = 1,5 mm) and stored at  $T = 37^{\circ}\text{C}$  and R.H. = 90% for 7 days, to allow cement's hardening. After this time, samples were sterilized by gamma irradiation (cobalt-60 at 25 kGy). Osteoblast-like cells MG63 (Istituto Zooprofilattico Sperimentale IZSLER, Brescia, Italy) were used. MG63 were expanded in DMEM medium (Dulbecco's Modified Eagle's Medium, Sigma, UK) supplemented with 10% FCS and antibiotics (100 U/mL penicillin, 100  $\mu\text{g/mL}$  streptomycin), then plated at a concentration of  $2 \times 10^4$  cells/well in 24-well plates containing sterile samples of experimental biomaterial and reference, and DMEM only without materials as internal control (CTR). Plates were cultured in standard conditions, at  $37 \pm 0.5^{\circ}\text{C}$  with 95% humidity and  $5\% \pm 0.2 \text{ CO}_2$  up to 7 days. Cell viability was measured after 3 and 7 days of culture by Alamar blue dye (Cell Viability Reagent, Life Technologies Corp., Oregon, USA): the reagent was added (1:10 v/v) to each well and incubated for

4 hours at 37°C. A redox indicator, incorporated in the reagent, changes its color in response to the chemical reduction of the medium resulting from living cells. The result is expressed as relative fluorescence units (RFU). The osteoblast viability was also calculated as percentage according to the following formula: cell viability % = OD sample / OD C<sub>Ba</sub> x 100, so referring the value of each sample to the reference material. Furthermore, both at 3- and 7-days supernatants from each well was collected and centrifuged to remove particulates and to measure Lactate Dehydrogenase (LDH detection kit, Roche diagnostics, IN, USA): enzyme released in medium when cell membrane is damaged. The test was performed following manufacturer's instruction and LDH concentration was spectrophotometrically read and reported in function of cell viability.

## **2.8. Gene expression analysis**

Gene expression of the most common markers of osteoblastic differentiation and activity was evaluated on all materials, as well as proinflammatory cytokines <sup>27</sup>. Total RNA was extracted from all samples at each experimental time using PureLink™ RNeasy Mini Kit (AMBION, Life Technologies, Carlsbad, CA, USA), quantified by NANODROP spectrophotometer (NANODROP 2720, Thermal Cycler, Applied Biosystem) and reverse transcribed with SuperScriptVILO cDNA Synthesis Kit (Life Technologies), following the manufacturer's instructions. The obtained cDNA of each sample was diluted to the final concentration of 5 ng/μL and semi-quantitative polymerase chain reaction (PCR) analysis was performed for each sample in duplicate in a LightCycler 2.0 Instrument (Roche Diagnostics GmbH, Mannheim, Germany) using QuantiTect SYBR Green PCR Kit (Qiagen, Hilden, Germany) and gene-specific primers (Table S2). The protocol included a denaturation cycle at 95°C for 15', 25 to 40 cycles of amplification (95°C for 15'', appropriate annealing temperature for each target for 20'', and 72°C for 20''). After melting curve analysis to check for amplicon specificity the threshold cycle was determined for each sample and relative gene expression was calculated using

the  $2^{-\Delta\Delta C_t}$  method<sup>27</sup>. For each gene, expression levels were normalized to GAPDH (glyceraldehyde 3-phosphate dehydrogenase) using C\_Ba as calibrator.

## 2.9. Immunoenzymatic analysis

Supernatants collected at 3 and 7 days were used for immunoenzymatic detection of Alkaline Phosphatase (ALP), Osteocalcin (OSTC), Interleukin 1 $\beta$  (IL1 $\beta$ ), Interleukin 6 (IL6) (ELISA kit, Finetest, Wuhan, China), and Type I Collagen (COL1, ELISA kit Biomatik Corp, Wilmington, USA). These proteins were quantified in duplicates for each sample, following customer instructions.

## 2.10. Statistical analysis

Statistical evaluation of data was performed using the software package SPSS/PC<sup>+</sup> Statistics<sup>TM</sup> 25.0 (SPSS Inc., Chicago, IL USA). The results presented are the mean of six independent values. Data are reported as mean  $\pm$  standard deviations (SD) at a significance level of  $p < 0.05$ . After having verified not normal distribution and homogeneity of variance by mean of Levene test, T2 Tamhane post-hoc test was performed to assess differences among groups.

## 3. Results

This study represents a first attempt to produce fibres-reinforced CPCs by self-assembling of fibres during cement hardening. The L-Dopa derivative gelator was chosen as LMWG due to its biocompatibility and ability to form fibres with high length/diameter ratio in the presence of calcium.

### 3.1 Rheological tests

A time sweep analysis was carried out to evaluate the ability of the pure Boc-L-Dopa(Bn)<sub>2</sub>-OH hydrogel to recover its shape and strength after fast spinning that transform the gel into sol.

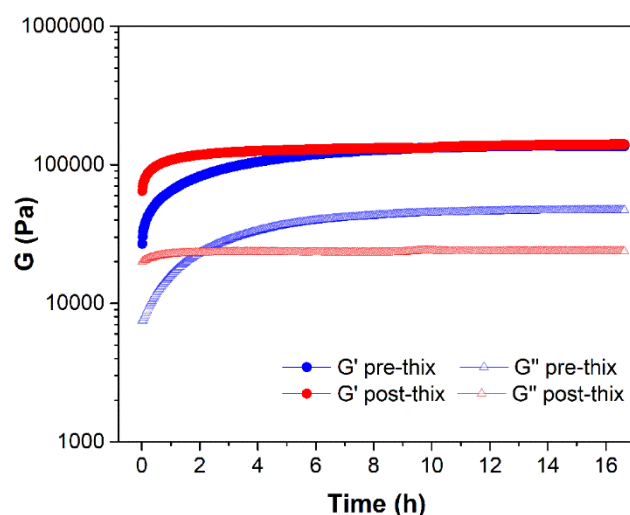


Figure 2. Time sweep of the hydrogel before (blue) and after (red) shaking the vial.

In Figure 2 the blue line corresponding to  $G'$  (obtained by the hydrogel analysis before shaking) is superimposable to the red one (obtained after shaking), thus confirming the good thixotropic properties of the hydrogel, a mandatory requirement for the fibres assembling inside the cement matrix. The analysis was performed only on the hydrogel at 2% w/v, as we analyzed a property independent from the concentration.

### 3.1.2. Fibre formation assessment

The LMWG used for cement's formulation can produce very long, thin and regular fibres (about 300 nm in diameter) forming a network in which they are strongly entangled (see Figure 3-a). No differences in the mean diameter values of the fibres obtained in cement samples at 1% and 2.6% have been observed (Figure S5).



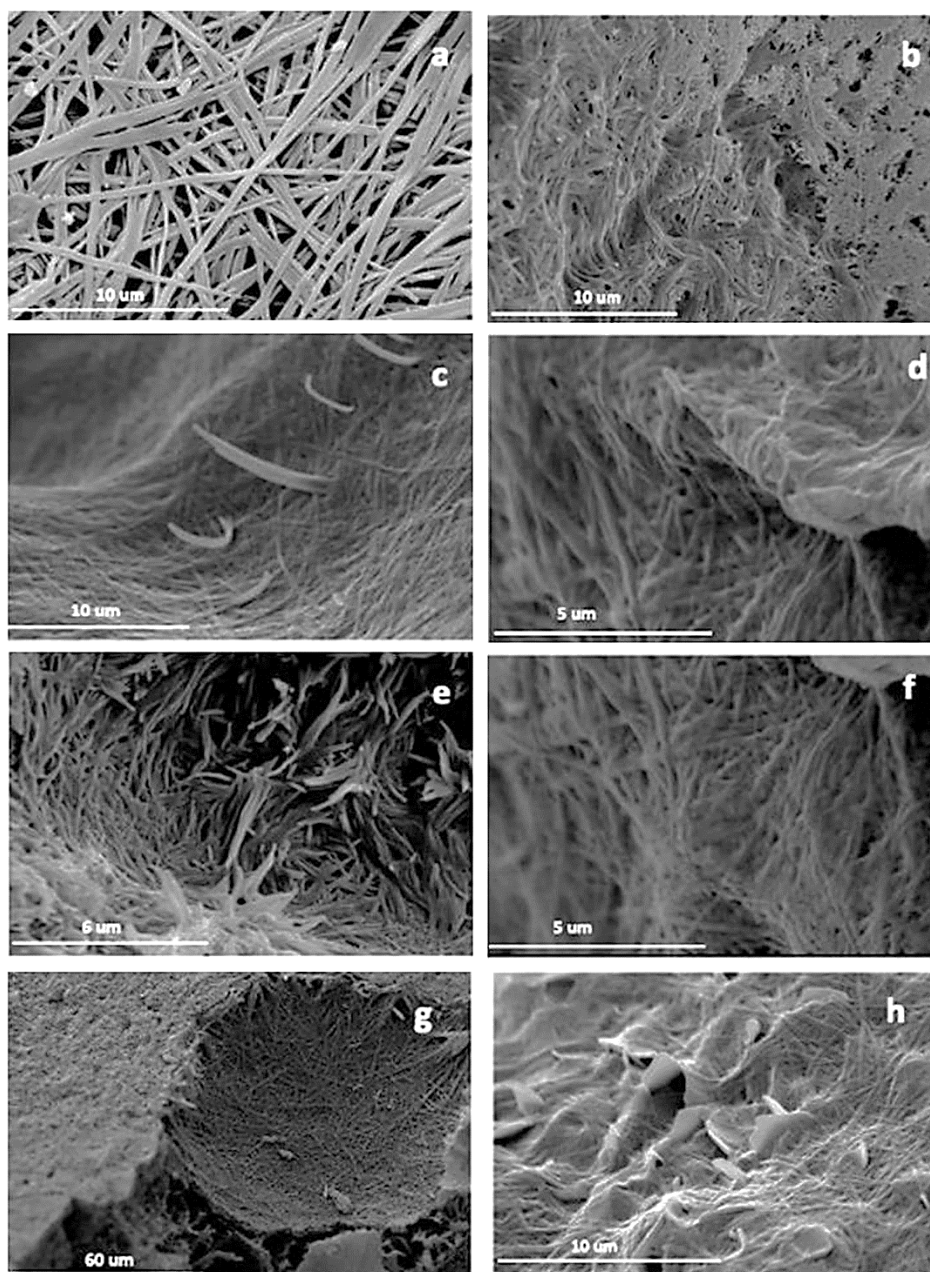


Figure 3. SEM images of the fibers obtained a) from the aqueous solution of the gelator used for the cement reinforcement at 1% w/w after air drying, and inside cement matrix of different compositions and after different hardening times: b) G1\_Ba after 20h of soaking in PB at 37°C; c,d) G1 after 7 days; e,f) G2.6 after 7 days; g,h) G1\_Ba and G2.6\_Ba after 7 days, respectively.

Since a self-assembling of fibres in such a dense matrix had not been previously obtained, a morphological characterization was carried out to demonstrate their actual formation. The



formation of fibres was monitored over time by immersing the cement sample in liquid nitrogen after set periods of soaking and collecting SEM images of the fractured surfaces.

The hydrogel formation usually takes place within few hours through the slow formation of fibers that entrap the solvent <sup>10</sup>. In particular, the formation of fibres in water takes about 16 hours to complete, as shown in Figure 3-a. Similarly, inside the cement the hydrogel takes up the same time to acquire the final morphology: in fact, the SEM analysis performed after 20 hours from the cement preparation revealed that the fibres formation inside the dense matrix was quite completed, as shown in Figure 3-b. For all the compositions enriched with the LMW gelator, the SEM images obtained from fractured surfaces after 7 days of soaking revealed a high number of fibres (see Figure 3-c,f) well distributed throughout the matrix and located mainly within the pores (see Figure 3-g) . Moreover, fibres appear strongly intertwined with each other (see Figure 3-d,f) and, most importantly, they show an excellent interaction with the platelets of the apatite phase (as visible in Figure 3-h), a crucial feature for the success of FRCPCs, as reported in literature <sup>28</sup>. However, on increasing hydrogel concentration a different fibres morphology has been evidenced: the presence of bushes of fibres, mainly located into pores, has been observed in cement G2.6 (see Figure 3-e) together with thin sheets of hydrogel.

### 3.2. Structural Characterization

XRD patterns of the gelator and of selected cement samples after 7 days of soaking are reported in

Figure 4-a, compared to the patterns of crystalline hydroxyapatite, alfa-TCP and barium sulphate, synthesized in our laboratory following the procedures reported in literature <sup>22,29</sup>.

To confirm the phase, collected diffractograms were superimposed to reference patterns from ICCD database: 00-009-0432 (hydroxyapatite), 00-009-0348 (alfa-TCP), 00-002-1199 (barium sulphate).

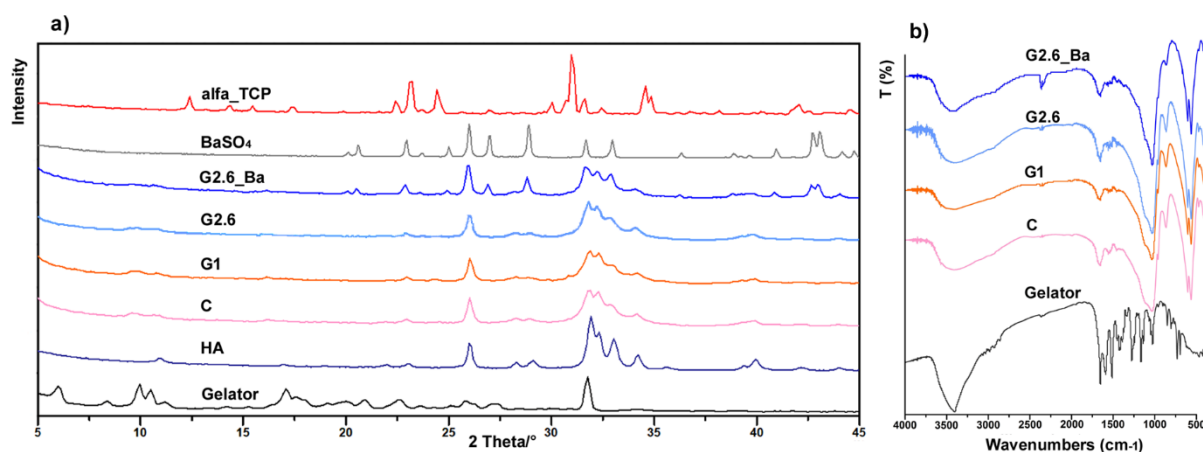


Figure 4. a) XRD diffraction patterns of the cements after 7 days of soaking compared to the reference patterns of hydroxyapatite (HA), alfa-TCP, gelator and BaSO<sub>4</sub> and b) FT-IR spectra of the obtained cements and of the gelator.

The presence of poorly crystalline hydroxyapatite obtained during cement's hardening is well evidenced by the broadening of the three most prominent reflections of hydroxyapatite, centered at 31.774, 32, 197 and 32,902 °/2 theta and corresponding to 211, 112 and 300 plane, respectively.

The reflections belonging to  $\alpha$ -TCP and DCPD are no longer present, confirming that after 7 days the phase conversion is complete and not affected by the presence of the gelator. Due to the low concentration of the gelator compared to the cement powders (both 1% and 2.6%) and to the overlap of more intense reflections belonging to hydroxyapatite, its main reflections are not visible in the XRD of the composite materials. The presence of BaSO<sub>4</sub>, added to obtain a radiopaque material<sup>30,31</sup>, did not interfere with the hardening reaction, as reported in literature<sup>18</sup>. The FT-IR spectra of the hardened pastes are reported in figure 4b: according to the X-rays patterns, infrared spectra are typical of a poorly crystalline hydroxyapatite. As a matter of fact, the absorption bands belonging to phosphate groups in the apatite matrix<sup>32</sup> (located at 550, 600, and 1070 cm<sup>-1</sup>) are very broad and those due to OH<sup>-</sup> stretching and libration modes, at 3572 and 630 cm<sup>-1</sup>, respectively, are no longer appreciable.

The distilled water used for the preparation of the soaking solutions was not decarbonated, and thus it contains carbonate ions, that can be easily incorporated into the structure of hydroxyapatite. IR spectra confirmed this finding. In fact, the characteristic bands of carbonate ions associated with the symmetric stretching mode at  $1450\text{ cm}^{-1}$  and the out of plane bending mode at  $870\text{ cm}^{-1}$  are clearly detectable in all the cement's formulations, thus evidencing the formation of a carbonated hydroxyapatite.

Furthermore, the characteristic bands of carbonate ions associated with the symmetric stretching mode at  $1450\text{ cm}^{-1}$  and the out of plane bending mode at  $870\text{ cm}^{-1}$  are clearly detectable in all the formulations, thus evidencing the formation of a carbonated hydroxyapatite. Two more bands typical of proteins, Amide I and Amide II, positioned at  $1530$  and  $1649\text{ cm}^{-1}$  are clearly visible in all IR spectra of the cement powders: their presence is ascribable to gelatin, added into the formulations of the starting powders. The presence of the hydrogel is not detectable, due to its low concentration.

### 3.3. Mechanical properties

Figure 5 illustrates the effect of fibre addition on the mechanical properties of the reinforced CPCs. No significant difference in compressive strength between reinforced cements containing the lowest amount of gelator and their reference samples was found. In contrast, G2.6 cements showed

higher stress values, significantly different when compared to all the formulations.

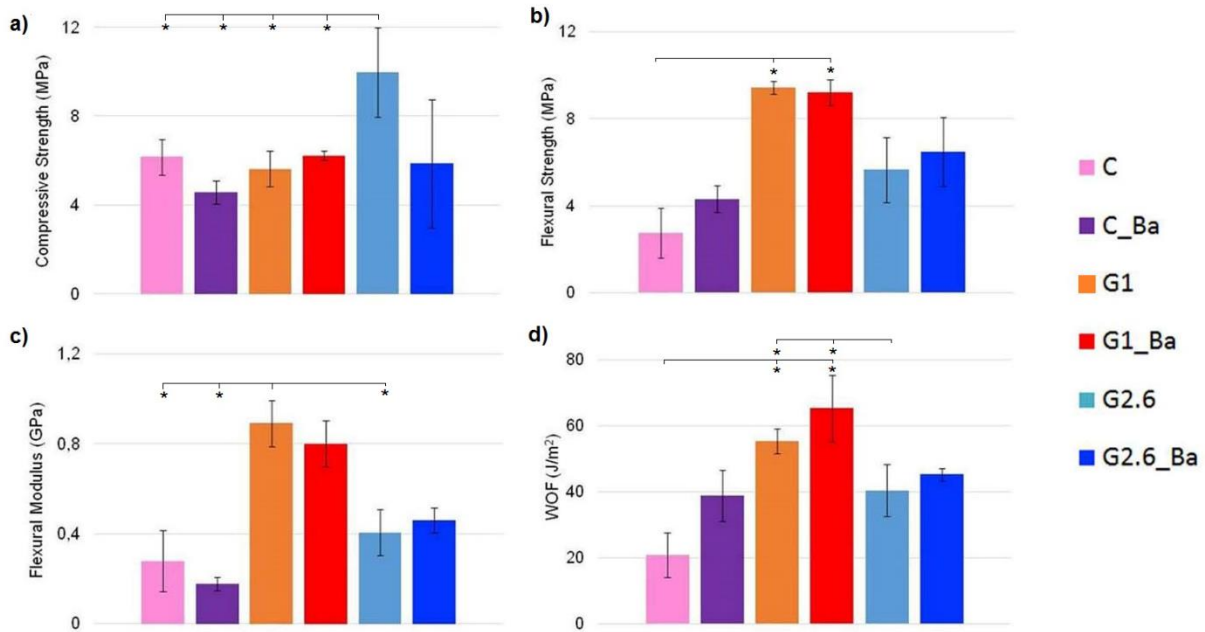


Figure 5. Mechanical properties of the obtained cements: a) Compressive Strength, b) Flexural Strength, c) Flexural Modulus and d) Work-Of-Fracture. Statistical analysis is reported in the figure (\*  $p < 0.05$ ):

a. Compressive Strength: \*G2.6 vs C, C\_Ba, G1, G1\_Ba;

b. Flexural Strength: \*C vs G1, G1\_Ba;

c. Flexural Modulus: \*G1 vs C, C\_Ba, G2.6;

d. Work of Fracture: \*C vs G1, G1\_Ba; \*G2.6 vs G1 and G1\_Ba

For the three-point bending tests the FRCPC sample bars were loaded to failure and the maximum flexural strength and modulus were calculated: the best performance was obtained from samples with 1% w/w of fibres, with flexural strength and modulus values 3,5 times higher than those of the reference samples (compare G1 and G1\_Ba with C). Even if the reinforcement effect of the gelator fibres on the Work-Of-Fracture is evident in all the formulations, a greater reinforcement was obtained from samples G1 and G1\_Ba compared to those containing 2.6% w/w of fibres.

### 3.4. Injectability tests

Since all the cements formulations showed a flowable consistency, the tests were carried out as reported in literature and maintaining the liquid to powder ratio of 0,52ml/g used for the pastes<sup>18</sup>.

Both Ba-containing formulations with 1% w/w and 2.6% w/w of fibres were tested and compared with their reference cement C\_Ba. The injectability curves obtained for the formulations C\_Ba, G1\_Ba and G2.6\_Ba are reported in Figure S6: each curve presents a very rapid increase of the load in the first millimeters of displacement, due to the critical force that must be applied to start the past flowing, and a subsequent plateau representing the load needed to maintain the flow. In the last portion of the curves, the load increases abruptly because of the mechanical contact between the plunger and the syringe's bottom when all the paste has been extruded.

The load required for cement extrusion (between 0,2- 0,3 kN) falls in the range useful for clinical applications<sup>33</sup>: the effect of gel addition produces just a low increase in the force needed to extrude the pasty material, in particular for G2.6\_Ba.

Excellent cohesion has been demonstrated by all formulations: the paste extruded in PB solution immediately after the preparation remained intact after 24 hours of immersion without any particle released to the surrounding medium (Figure S7).

### 3.5. Micro-CT Characterization

Micro-CT analysis (Figure 6) showed that the presence of the fibres did not affect the overall porosity in G1 and G2.6 samples, with average values comparable to control sample (8.6% vs 8.1% porosity).

The addition of barium appeared to reduce the porosity regardless of the presence of the fibres (4.3% averaging on C\_Ba, G1\_Ba and G2.6\_Ba). Interestingly, differences between the pore's diameter distribution were found: in fact, while the most diffuse pore size in sample C is between 0-50  $\mu\text{m}$ , it increased up to 200  $\mu\text{m}$  in the other samples, highlighting that the presence of fibres and/or barium shifted the pore diameters towards bigger values. In particular, a higher number of pores with diameters between 0-100  $\mu\text{m}$  was found in G1 sample.

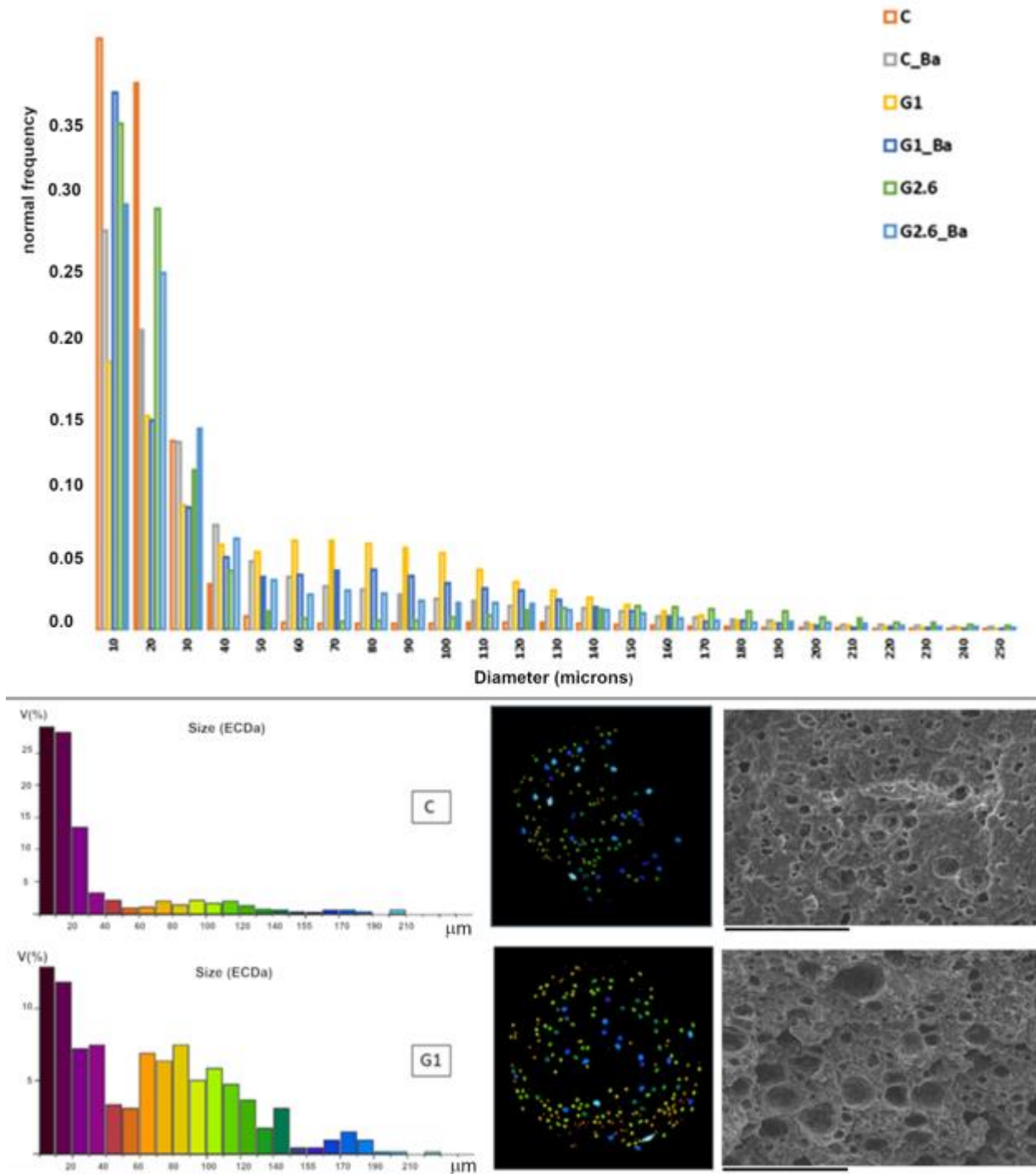


Figure 6. Above, histogram representing the closed pores distribution of the obtained cements: pore's diameter is calculated as Volume-equivalent sphere diameter (ESDv). Below, examples of micro-CT sections for cement C and G1 with colour histogram and map of pores sizes, calculated as Average object area-equivalent circle diameter (ECDA), as screened in "CT-Analyser" software, together with the respective scanning electron micrographs (scale bar =200 microns)

### 3.6. *In vitro* biocompatibility

To assess the biological safety of the materials, in accordance with their nature and duration of contact with human tissues, different biocompatibility tests must be performed. First, the cell viability has been quantitatively assessed considering a reduction by more than 30% in comparison to reference sample (C\_Ba) as a consequence of a cytotoxic effect, then the lactate dehydrogenase (LDH) in supernatant has been measured, since it is known that the release of this enzyme is a sign of cell membranes damage (UNI EN ISO 10993-5:2009). The viability of MG63 was measured after 3 and 7 days of culture (Figure 7-a).

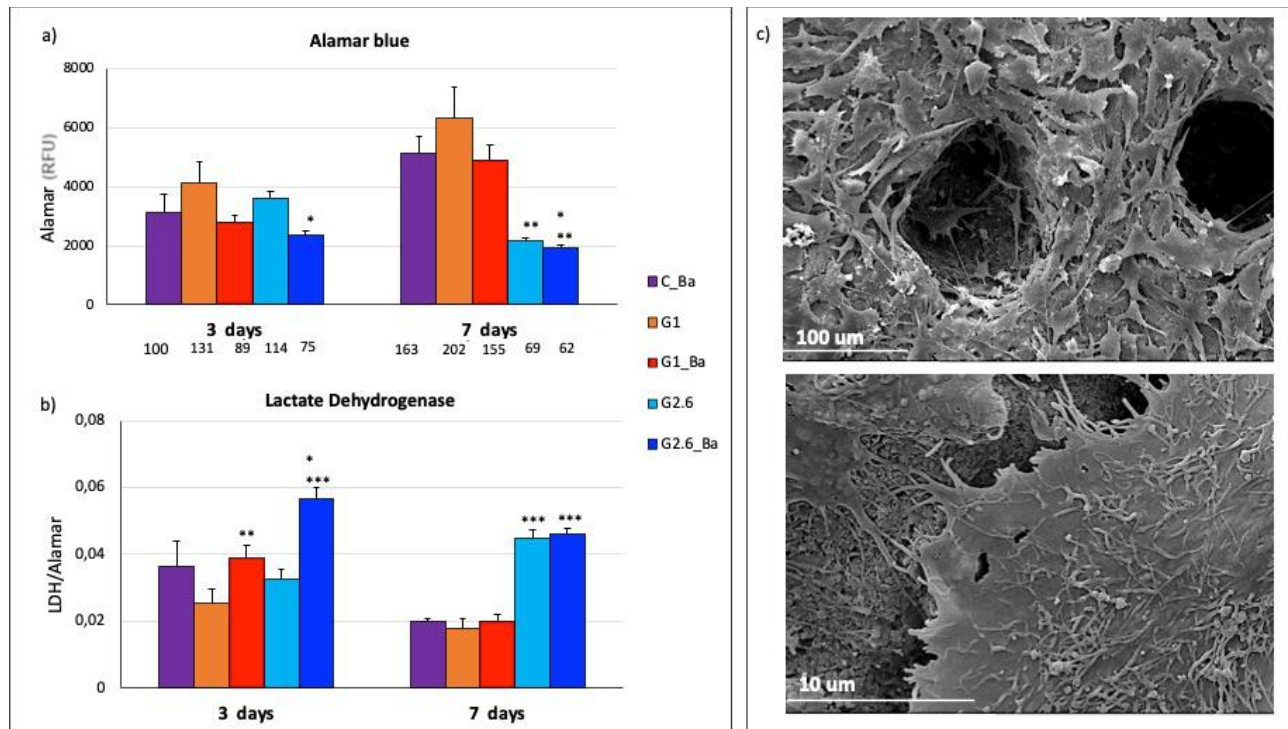


Figure 7. a) MG63 osteoblast viability (Alamar Blue test), b) LDH release in supernatant (biochemical test) after 3 and 7 days of culture in standard conditions with experimental and reference samples and c) SEM images of cells grown on sample G1. Percentage of viability is indicated under each column in graph a).

Statistical analysis is reported in the figure (\* $p < 0.05$ , \*\* $p < 0.005$ , \*\*\* $p < 0.0005$ ).

- Alamar Blue 3 days: \*G2.6\_Ba vs G1, G1\_Ba, G2.6; 7 days: \*\*G2.6, G2.6\_Ba vs C\_Ba, G1, G1\_Ba; \*G2.6\_Ba vs G2.6.
- LDH 3 days: \*\*G1\_Ba vs G1; \*G2.6\_Ba vs C\_Ba; \*\*\*G2.6\_Ba vs G1, G1\_Ba, G2.6; 7 days: \*\*\*G2.6, G2.6\_Ba, vs C\_Ba, G1, G1\_Ba.

At 3 days no differences were found among experimental samples and reference, apart from G2.6\_Ba, whose values were significantly lower than other materials. At 7 days viability of C\_Ba, G1, and G1\_Ba was significantly improved when compared to 3 days values ( $p < 0.0005$ ,  $p < 0.005$ ,  $p < 0.0005$ , respectively. Data not shown). On the contrary, viability of both G2.6 and G2.6\_Ba was significantly lower when compared to C\_Ba, G1, G1\_Ba with values lower than 70% (69% and 63% for G2.6 and G2.6\_Ba, respectively), revealing cytotoxicity. This phenomenon should be probably ascribed to the tendency of Boc-L-Dopa(Bn)<sub>2</sub>-OH to form precipitates at higher concentrations. These aggregates are visible by SEM analysis (Figure 3-e) and hardly breakable, thus resulting in an environment less favourable for cell growth. Therefore, the preferred gelator concentrator is 1% as it ensures the formation of a strong fibers network (Figure 3 c-d), leading to the formation of thixotropic hydrogels, without the formation of unsafe precipitates.

LDH results are shown in figure 7b. The release of LDH in medium is due to damage of cell membrane and it reached significant higher values in G1\_Ba and G2.6\_Ba in comparison to other groups at 3 days. At 7 days C\_Ba, G1, and G1\_Ba values decreased; on the contrary, both G2.6 and G2.6\_Ba showed a significant higher release of LDH. These results were strictly inversely correlated with viability data (Pearson -0,873,  $p < 0,0005$ ).

### 3.7. Gene expression

The analyses of representative markers of osteoblast activity and differentiation and of microenvironment inflammation were performed on MG63 after 7 days of culture on C\_Ba, G1, and G1\_Ba materials. G2.6 and G2.6\_Ba were excluded as the samples had previously showed typical signs of cytotoxicity. Furthermore, the poor amount of extracted RNA from G2.6 and G2.6\_Ba, not suitable to correctly carry out the subsequent analyses of gene expression, confirmed the scarcity of cells on these samples. Gene expression is reported in Figure 8a-f. No differences among groups were found for ALPL and BGALP (Figure 8-a,c). Referring to these genes, G1\_Ba was similar to G1



and C\_Ba, demonstrating that these materials did not affect osteoblast differentiation and mineralization. COL1A1 and SPARC expression (Figure 8-b,d) was significantly upregulated in G1\_Ba when compared to G1 sample gene expression and reached level similar to C\_Ba. IL1 $\beta$  and IL6 are pro-inflammatory cytokines involved in the process of bone formation, and they have a relevant role in osteoblast and osteoclast differentiation. In the present study, regarding IL1 $\beta$  expression, no differences were found among groups. IL6 was significantly over-expressed in G1, when compared to both C\_Ba and G1\_Ba. G1\_Ba was not different from C\_Ba (Figure 8-e,f).

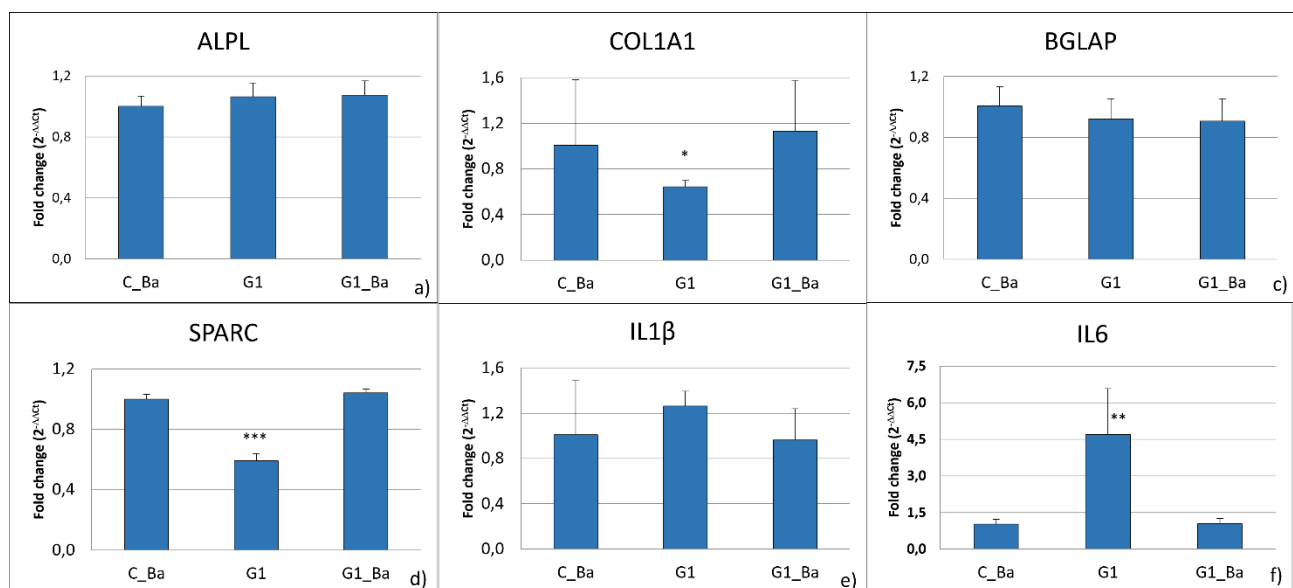


Figure 8. Gene expression of osteoblast after 7 days of culture by RT-PCR. Some representative markers of osteoblast differentiation and activity (a-d) and proinflammatory reaction (e-f) are shown. Results were normalized to GAPDH expression and data are given as fold change relative to the reference group (C\_Ba), considered as 1. Results are the main (+/- SD) of six replicates. Statistical analysis is reported in the figure (\* $p < 0.05$ , \*\* $p < 0.005$ , \*\*\* $p < 0.0005$ ):

- b. COL1A1: \*G1 vs G1\_Ba;
- d. SPARC: \*\*\*G1 vs C\_Ba, G1\_Ba;
- f. IL6: \*\*G1 vs C\_Ba, G1\_Ba

### 3.8 Immunoenzymatic analysis

The evaluation of ALP, COL1 and OSTC by immunoenzymatic method (Figure 9a-c) revealed analogous behaviour among the 3 materials evaluated, similarly to what observed as gene expression at 7 days of culture. OSTC values were significantly higher in C\_Ba in comparison with G1

and G1\_Ba ( $p < 0.05$ ) and G1 was higher than G1\_Ba ( $p < 0.005$ ) at 3 days of culture, but at 7 days the differences were no longer significant. All markers showed much higher values at 7 days than at 3 days in all groups, demonstrating the growing activity of osteoblasts during the culture time and the maintenance of cell differentiation. The measure of inflammatory cytokine IL1 $\beta$  revealed no differences of production among groups at both experimental times. Conversely, the measurement of IL6 demonstrated a significant difference between G1\_Ba and C\_Ba at 3 days ( $p < 0.0005$ ) and between G1 and C\_Ba at 7 days ( $p < 0.005$ ), although the quantification of this interleukin in all groups was low at 3 days (below 3 pg/ml) and the values fell, being barely detected, at 7 days (below 0.1 pg/mL) as evidenced in Figure 9 d-e.

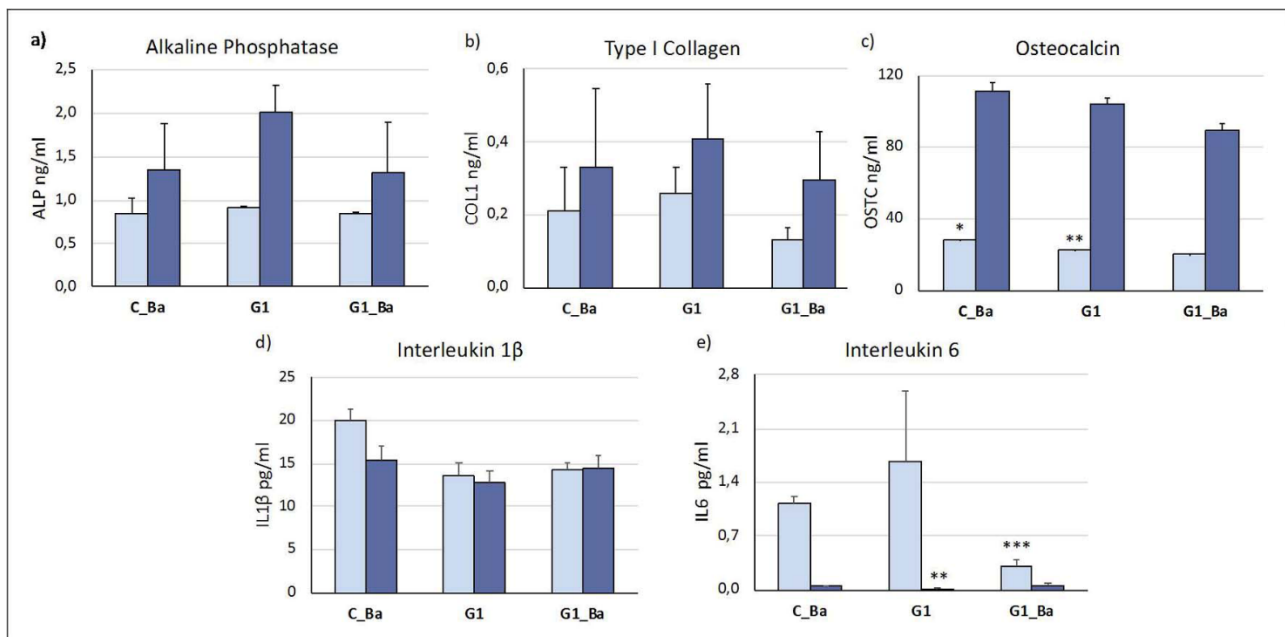


Figure 9. Protein release detected by ELISA assay after 3 (light blue) and 7 (blue) days of culture. Some representative markers of osteoblast differentiation and activity and proinflammatory reaction are shown. Results are the mean (+/- sd) of six replicates. Statistical analysis is reported in the figure (\* $p < 0.05$ , \*\* $p < 0.005$ , \*\*\* $p < 0.0005$ ):

c. Osteocalcin 3 days: \*C\_Ba vs G1, G1\_Ba; \*\*G1 vs G1\_Ba;

e. IL6 3 days: \*\*\* G1\_Ba vs C\_Ba; 7 days: \*\* G1 vs C\_Ba

#### 4. Discussion

Several strategies have been evaluated to reinforce CPC: in particular, the addition to the cement powders of preformed fibres of different lengths, materials and aspect/ratios to enhance

mechanical properties and fibres-matrix adhesion has been studied <sup>6</sup>. To the best of our knowledge, our paper represents the first attempt to produce fibres-reinforced calcium phosphate cements by self-assembling of fibres during cement hardening. To obtain this goal, a L-Dopa derivative gelator was chosen as LMWG, since it is biocompatible and able to form fibres in the presence of calcium. The formation of fibres in aqueous solutions usually starts soon after the addition of the trigger ( $\text{CaCl}_2$ ) and up to 16 hours are required to obtain the final morphology: obtained fibres are about 300 nm wide and up to 1000 micron long and they form a well interconnected network (Figure 3-a). The rheological characterization of the hydrogel by means of time sweep experiments demonstrated the hydrogel thixotropy, that is the ability to perfectly recover its mechanical properties after break, a needful feature for the present work. FRCPCs were obtained by introducing two different concentrations of hydrogel, 1% and 2.6% w/w, as liquid phase in the cement matrix. Given the high liquid/powder ratio used to obtain injectable compositions, 40 minutes are needed for the initial setting times, when measured with a Gillmore device. Morphological examination carried out on the fracture surfaces of all the sample demonstrated the ability of the hydrogel to form fibres within 20 hours even when mixed with a huge amount of powders for both the cements formulations. Fibres appeared similar for shape and size to those obtained in aqueous solution (compare Figure 3 a-f), even if a lower reproducibility was found in the morphology of the fibres produced with the higher hydrogel amount (Figure 3-e). The extent of conversion of the starting phosphates into hydroxyapatite was evaluated by X-ray diffraction patterns. For all the samples, the hardening reaction is complete after 7 days and it is not affected by the presence of the gelator nor barium sulfate. The results of the mechanical characterization suggest that fibre reinforcement has a more pronounced effect when cements are tested in bending than in compression <sup>34</sup>. The presence of fibres entangled with the inorganic phase strongly enhanced the flexural strength of G1 and G1\_Ba cements: recorded values are nearly doubled with respect to the unreinforced cements C

and C\_Ba. A similar trend is observed for flexural modulus, where the cements containing the lower amount of gel exhibited the greatest improvement of about three-fold compared to the corresponding fibres-free CPCs. The work of fracture (and hence the toughness) was improved of about three-fold, even if values are lower than those reported in literature, mostly due to the high L/P (liquid/powder) ratio used here to obtain an injectable cement and to the fibres dimensions and composition. These results demonstrate the effective reinforcement of the fibres entangled with the cement matrix: in particular, it is important to emphasize that the three-fold increase of mechanical properties is obtained by a quite low amount (1%wt) of thin fibres (about 1000 micron x 300 nm), with respect to the values reported in literature. For example, addition of Poly(vinyl alcohol) fibres of different length (ranging from 3 to 6 mm), different diameters (from 26 to 14 microns) and in different amount (2.5 and 5% w/w) to  $\alpha$ -TCP powders as starting material for an apatite-forming cement, improved more than 2-fold the flexural strength, and highlighted the prominent effect of concentration with respect to the fibre length <sup>34</sup>. Several papers reported the addition of Poly(l-lactide-co-glycolide) acid (PLGA) fibres both to apatite and to brushite-forming cements. In particular, the paper of Maenz et al.<sup>35</sup> evaluated the properties of injectable brushite cements enriched by PLGA fibres (diameter of 25 microns) as a function of their weight and length: only with a 5% (w/w) of 1mm-long fibres a significant (>25%) enhancement of the flexural strength can be obtained.

Therefore, the reinforcement observed in our cements could be due both to the nature of the self-assembled fibres, which demonstrated a high affinity for the apatite phase, and to their very high length/diameter ratio, important features for a successful fibre-reinforcement <sup>36</sup>.

Generally, the presence and size of pores decrease strength and elastic modulus <sup>37–39</sup>.

Microtomographic analyses revealed an increased pores size distribution in G1 and G1\_Ba: despite the increasing of pores size around and beyond 100  $\mu$ m, fibres were able to enhance mechanical

performances of composite cements. Pore size of at least 100  $\mu\text{m}$  is also beneficial for cell growth. Used spatial resolution did not permitted to investigate pores below 5  $\mu\text{m}$  of diameter, potentially important in the mesoporous structure of CPCs. To overcome this limitation, techniques such as Brunauer-Emmett-Teller (BET) and mercury intrusion porosimetry (MIP) should be integrated. However, from the biological point of view, pore size is beneficial for cell growth when above 100  $\mu\text{m}$ <sup>40–43</sup>. Preliminary assays of cytotoxicity were performed, followed by a more in-depth analysis of the selected materials by gene expression and protein release<sup>44,45</sup>. Cell viability test of the cements G2.6 and G2.6\_Ba showed low values, in particular after 7 days of culture, revealing cell damage as confirmed by LDH dosage. The mechanical properties and pores size distribution matched very well to what observed by preliminary biological test and led to identify as most promising materials G1 and G1\_Ba. On these materials the expression of some keys genes normally evaluated as osteogenic activity<sup>46</sup> has been performed. The analysis highlighted a similar expression level among the materials. ALPL, COL1A1, SPARC and BGLAP, genes that encode for alkaline phosphatase, collagen type I, osteonectin and osteocalcin, respectively, are known to be expressed in different phases of the osteoblast's activity. By a further analysis (not shown) emerged a more abundant expression of SPARC and COL1A1 at this culture endpoint, thus revealing an intermediate stage of osteogenesis, already involving the mineralization phase. In fact, type I collagen represents the major component of the bone extracellular matrix, whose deposition is regulated also by osteonectin, which has high Ca affinity and contribute with collagen to form the matrix and to mineralize it<sup>47</sup>. Most importantly, the protein quantification confirmed what observed by molecular biology: at 7 days of culture, similar amount of ALP, type I COLL and OSTC were detected in supernatants of all materials. The strong increase over time of proteins connected to osteoblast's activity pointed out the positive stimulating effect of G1 and G1\_Ba. Finally, IL1 $\beta$  and IL6 were quantified to exclude possible

inflammatory effects elicited by the materials <sup>48</sup>. IL1 $\beta$  did not differ in experimental and reference materials, and IL6 was expressed at negligible levels, so not adversely affecting osteoblast activity. Injectability of CPCs is a key feature for minimally invasive surgical techniques, especially when defects have limited accessibility and when there is the need to conform to a defect area of complex shape. For all the samples tested, the stress values required to extrude the dough were in the good range to ensure the ease of injection <sup>49</sup>. Furthermore, the cement maintained a good cohesion even after 24 hours of immersion in PB. No evidence of phase separation, which is a major issue inhibiting successful delivery of injectable CPC, was found in the extruded samples.

## **5. Conclusions**

After several attempts, an efficient method for the preparation of an injectable FRCPC for bone regeneration was developed. Supramolecular fibres formed by LMWG self-assembling were grown for the first time inside a calcium phosphate bone cement using calcium ions as trigger, and provided structural and mechanical support to the material. A 1% w/w ratio between the gelator and the cement powders and a L/P ratio of 0.52 mL/g ensured the formation of a great number of fibres, which were clearly visible from SEM images. The fibres were homogeneously dispersed all over the matrix and mainly located inside pores, guaranteeing a reinforcement effect even if they promoted the formation of a higher number of pores larger than 100 $\mu$ m when compared with the reference cements.

The formulations containing 1% w/w of fibres were biocompatible and able to support a correct osteoblast activity in terms of main bone markers, without inducing inflammation. The increase of the anabolic markers and the decrease of ILs over the time suggest an osteoblast growth in presence of these materials, similar for innovative and known materials. The development of FRCPCs in combination with LMWGs opens the possibility to produce a whole new class of bone cements.

Moreover, the peptidic nature of the gelator makes it possible to modify its structure and functionalize it covalently with bioactive molecules and drugs.

## Acknowledgments

This work was partly supported by the Project “5×1000” 2019: “Medicina Rigenerativa e Riparativa Personalizzata per le Patologie dei Tessuti Muscolo-Scheletrici e La Chirurgia Ricostruttiva Ortopedica”.

The Authors wish to thank Dr. Paola Torricelli for her precious contribution in setting up the experiments and processing the results.

## Data availability

The raw/processed data required to reproduce these findings cannot be shared at this time as the data also forms a part of an ongoing study.

## References

- (1) Brown, W.E. and Chow, L. C. A New Calcium Phosphate Water-Setting Cement. In *Cements Research Progress*; Brown, W. E., Ed.; Westerville, 1986; pp 352–379.
- (2) Bohner, M.; Gbureck, U.; Barralet, J. E. Technological Issues for the Development of More Efficient Calcium Phosphate Bone Cements: A Critical Assessment. *Biomaterials* **2005**, *26* (33), 6423–6429, DOI:10.1016/j.biomaterials.2005.03.049.
- (3) Von Gonten, A. S.; Kelly, J. R.; Antonucci, J. M. Load-Bearing Behavior of a Simulated Craniofacial Structure Fabricated from a Hydroxyapatite Cement and Bioresorbable Fiber-Mesh. *J. Mater. Sci. Mater. Med.* **2000**, *11* (2), 95–100, DOI:10.1023/A:1008992900829.
- (4) Beaudoin, J. J. *Handbook of Fiber-Reinforced Concrete: Principles, Properties, Developments and Applications*; Noyes Publications: Park Ridge, N.J., 1990.
- (5) Nabi Saheb, D.; Jog, J. P. Natural Fiber Polymer Composites: A Review. *Adv. Polym. Technol.* **1999**, *18* (4), 351–363, DOI:10.1002/(SICI)1098-2329(199924)18:4<351::AID-ADV6>3.0.CO;2-X.
- (6) Canal, C.; Ginebra, M. P. Fibre-Reinforced Calcium Phosphate Cements: A Review. *J. Mech. Behav. Biomed. Mater.* **2011**, *4* (8), 1658–1671, DOI:10.1016/j.jmbbm.2011.06.023.
- (7) Krüger, R.; Groll, J. Fiber Reinforced Calcium Phosphate Cements - On the Way to Degradable Load Bearing Bone Substitutes? *Biomaterials* **2012**, *33* (25), 5887–5900, DOI:10.1016/j.biomaterials.2012.04.053.
- (8) Callister, W. D.; Rethwisch, D. G. *Materials Science and Engineering: An Introduction (2nd Edition)*, 8th ed.; John Wiley & Sons, Inc., 1991; Vol. 12 DOI:10.1016/0261-3069(91)90101-9.
- (9) Draper, E. R.; Adams, D. J. Low-Molecular-Weight Gels: The State of the Art. *Chem* **2017**, *3* (3), 390–410, DOI:10.1016/j.chempr.2017.07.012.
- (10) Giuri, D.; Jurković, L.; Fermani, S.; Kralj, D.; Falini, G.; Tomasini, C. Supramolecular Hydrogels

- with Properties Tunable by Calcium Ions: A Bio-Inspired Chemical System. *ACS Appl. Bio Mater.* **2019**, 2 (12), 5819–5828, DOI:10.1021/acsabm.9b00828.
- (11) Zanna, N.; Focaroli, S.; Merlettini, A.; Gentilucci, L.; Teti, G.; Falconi, M.; Tomasini, C. Thixotropic Peptide-Based Physical Hydrogels Applied to Three-Dimensional Cell Culture. **2021**, 13, 10, DOI:10.1021/acsomega.7b00322.
  - (12) Chen, L.; Mcdonald, T. O.; Adams, D. J. Salt-Induced Hydrogels from Functionalised-Dipeptides3. **2013**, 3, 8714, DOI:10.1039/c3ra40938d.
  - (13) Chen, L.; Pont, G.; Morris, K.; Lotze, G.; Squires, A.; Serpell, L. C.; Adams, D. J. Salt-Induced Hydrogelation of Functionalised-Dipeptides at High PH. *Chem. Commun.* **2011**, 47 (44), 12071–12073, DOI:10.1039/c1cc15474e.
  - (14) Mcewen, H.; Du, E. Y.; Mata, J. P.; Thordarson, P.; Martin, A. D. Tuning Hydrogels through Metal-Based Gelation Triggers †. *J. Mater. Chem. B* **2017**, 5, 9412, DOI:10.1039/c7tb02140b.
  - (15) Giuri, D.; Ravarino, P.; Tomasini, C. L-Dopa in Small Peptides: An Amazing Functionality to Form Supramolecular Materials. *Org. Biomol. Chem.* **2021** DOI:10.1039/d1ob00378j.
  - (16) Du, X.; Zhou, J.; Shi, J.; Xu, B. Supramolecular Hydrogelators and Hydrogels: From Soft Matter to Molecular Biomaterials. *Chem. Rev.* **2015**, 115 (24), 13165–13307, DOI:10.1021/acs.chemrev.5b00299.
  - (17) Knani, D. Low Molecular Weight Hydro-and Organo Gelators Used for Medical Applications. *Biomed. J. Sci. Tech. Res.* **2019**, 12 (5), 9553–9554, DOI:10.26717/BJSTR.2019.12.002315.
  - (18) Di Filippo, M. F.; Dolci, L. S.; Albertini, B.; Passerini, N.; Torricelli, P.; Parrilli, A.; Fini, M.; Bonvicini, F.; Gentilomi, G. A.; Panzavolta, S.; Bigi, A. A Radiopaque Calcium Phosphate Bone Cement with Long-Lasting Antibacterial Effect: From Paste to Injectable Formulation. *Ceram. Int.* **2020** DOI:10.1016/j.ceramint.2019.12.272.
  - (19) Zanna, N.; Iaculli, D.; Tomasini, C. Organic & Biomolecular Chemistry The Effect of L-DOPA Hydroxyl Groups on the Formation of Supramolecular Hydrogels †. *Org. Biomol. Chem.* **2017**, 15, 5797, DOI:10.1039/c7ob01026e.
  - (20) Gaucher, A.; Dutot, L.; Barbeau, O.; Hamchaoui, W.; Wakselman, M.; Mazaleytrat, J. P. Synthesis of Terminally Protected (S)-B3-H-DOPA by Arndt-Eistert Homologation: An Approach to Crowned  $\beta$ -Peptides. *Tetrahedron Asymmetry* **2005**, 16 (4), 857–864, DOI:10.1016/j.tetasy.2004.11.089.
  - (21) Panzavolta, S.; Torricelli, P.; Bracci, B.; Fini, M.; Bigi, A. Functionalization of Biomimetic Calcium Phosphate Bone Cements with Alendronate. *J. Inorg. Biochem.* **2010**, 104 (10), 1099–1106, DOI:10.1016/j.jinorgbio.2010.06.008.
  - (22) Bigi, A.; Bracci, B.; Panzavolta, S. Effect of Added Gelatin on the Properties of Calcium Phosphate Cement. *Biomaterials* **2004**, 25 (14), 2893–2899, DOI:10.1016/J.BIOMATERIALS.2003.09.059.
  - (23) Bigi, A.; Panzavolta, S.; Rubini, K. Setting Mechanism of a Biomimetic Bone Cement. *Chem. Mater.* **2004**, 16 (19), 3740–3745, DOI:10.1021/CM049363E/ASSET/IMAGES/LARGE/CM049363EN00001.JPEG.
  - (24) Vallo, C. I. Influence of Load Type on Flexural Strength of a Bone Cement Based on PMMA. *Polym. Test.* **2002**, 21 (7), 793–800, DOI:10.1016/S0142-9418(02)00013-2.
  - (25) Dunne, N. J.; Orr, J. F. Influence of Mixing Techniques on the Physical Properties of Acrylic Bone Cement. *Biomaterials* **2001**, 22 (13), 1819–1826, DOI:10.1016/S0142-9612(00)00363-X.
  - (26) Tadier, S.; Galea, L.; Charbonnier, B.; Baroud, G.; Bohner, M. Phase and Size Separations Occurring during the Injection of Model Pastes Composed of  $\beta$ -Tricalcium Phosphate Powder, Glass Beads and Aqueous Solutions. *Acta Biomater.* **2014**, 10 (5), 2259–2268, DOI:10.1016/j.actbio.2013.12.018.
  - (27) Schmittgen, T. D.; Livak, K. J. Analyzing Real-Time PCR Data by the Comparative CT Method.



*Nat. Protoc.* **2008**, 3 (6), 1101–1108, DOI:10.1038/NPROT.2008.73.

- (28) Gallinetti, S.; Mestres, G.; Canal, C.; Persson, C.; Ginebra, M. P. A Novel Strategy to Enhance Interfacial Adhesion in Fiber-Reinforced Calcium Phosphate Cement. *J. Mech. Behav. Biomed. Mater.* **2017**, 75 (August), 495–503, DOI:10.1016/j.jmbbm.2017.08.017.
- (29) Bertoni, E.; Bigi, A.; Cojazzi, G.; Gandolfi, M.; Panzavolta, S.; Roveri, R. Nanocrystals of Magnesium and Fluoride Substituted Hydroxyapatite. *J. Inorg. Biochem.* **1998**, 72, 29–35, .
- (30) Ginebra, M. P.; Albuixech, L.; Fernández-Barragán, E.; Aparicio, C.; Gil, F. J.; San Román, J.; Vázquez, B.; Planell, J. A. Mechanical Performance of Acrylic Bone Cements Containing Different Radiopacifying Agents. *Biomaterials* **2002**, 23 (8), 1873–1882, DOI:10.1016/S0142-9612(01)00314-3.
- (31) Fang, C.; Hou, R.; Zhou, K.; Hua, F.; Cong, Y.; Zhang, J.; Fu, J.; Cheng, Y. J. Surface Functionalized Barium Sulfate Nanoparticles: Controlled in Situ Synthesis and Application in Bone Cement. *J. Mater. Chem. B* **2014**, 2 (9), 1264–1274, DOI:10.1039/c3tb21544j.
- (32) Hesarakı, S.; Alizadeh, M.; Borhan, S.; Pourbaghi-Masouleh, M. Polymerizable Nanoparticulate Silica-Reinforced Calcium Phosphate Bone Cement. *J. Biomed. Mater. Res. - Part B Appl. Biomater.* **2012**, 100 B (6), 1627–1635, DOI:10.1002/jbm.b.32731.
- (33) Jansen, J.; Ooms, E.; Verdonchot, N.; Wolke, J. Injectable Calcium Phosphate Cement for Bone Repair and Implant Fixation. *Orthop. Clin. North Am.* **2005**, 36 (1), 89–95, DOI:10.1016/j.ocl.2004.06.014.
- (34) Kucko, N. W.; De Lacerda Schickert, S.; Sobral Marques, T.; Herber, R. P.; Van Den Beuken, J. J. P.; Zuo, Y.; Leeuwenburgh, S. C. G. Tough and Osteocompatible Calcium Phosphate Cements Reinforced with Poly(Vinyl Alcohol) Fibers. *ACS Biomater. Sci. Eng.* **2019**, 5 (5), 2491–2505, DOI:10.1021/acsbmaterials.9b00226.
- (35) Maenz, S.; Kunisch, E.; Mühlstädt, M.; Böhm, A.; Kopsch, V.; Bossert, J.; Kinne, R. W.; Jandt, K. D. Enhanced Mechanical Properties of a Novel, Injectable, Fiber-Reinforced Brushite Cement. *J. Mech. Behav. Biomed. Mater.* **2014**, 39, 328–338, DOI:10.1016/j.jmbbm.2014.07.028.
- (36) Castro, A. G. B.; Polini, A.; Azami, Z.; Leeuwenburgh, S. C. G.; Jansen, J. A.; Yang, F.; van den Beuken, J. J. P. Incorporation of PLLA Micro-Fillers for Mechanical Reinforcement of Calcium-Phosphate Cement. *J. Mech. Behav. Biomed. Mater.* **2017**, 71 (March), 286–294, DOI:10.1016/j.jmbbm.2017.03.027.
- (37) Marchiori, G.; Berni, M.; Boi, M.; Petretta, M.; Grigolo, B.; Bellucci, D.; Cannillo, V.; Garavelli, C.; Bianchi, M. Design of a Novel Procedure for the Optimization of the Mechanical Performances of 3D Printed Scaffolds for Bone Tissue Engineering Combining CAD, Taguchi Method and FEA. *Med. Eng. Phys.* **2019**, 69, 92–99, DOI:10.1016/j.medengphy.2019.04.009.
- (38) Liu, D. M. Influence of Porosity and Pore Size on the Compressive Strength of Porous Hydroxyapatite Ceramic. *Ceram. Int.* **1997**, 23 (2), 135–139, DOI:10.1016/S0272-8842(96)00009-0.
- (39) Liu, D.; Šavija, B.; Smith, G. E.; J Flewitt, P. E.; Lowe, T.; Schlangen, E.; Liu, D.; Smith, G. E.; J Flewitt, P. E.; Šavija, B.; Schlangen Microlab, E.; Lowe, T. Towards Understanding the Influence of Porosity on Mechanical and Fracture Behaviour of Quasi-Brittle Materials: Experiments and Modelling. **2017**, 205, 57–72, DOI:10.1007/s10704-017-0181-7.
- (40) Mandal, B. B.; Kundu, S. C. Cell Proliferation and Migration in Silk Fibroin 3D Scaffolds. *Biomaterials* **2009**, 30 (15), 2956–2965, DOI:10.1016/j.biomaterials.2009.02.006.
- (41) Lee, H.; Hwang, H.; Kim, Y. S.; Jeon, H.; Kim, G. H. Physical and Bioactive Properties of Multi-Layered PCL/Silica Composite Scaffolds for Bone Tissue Regeneration. *Chem. Eng. J.* **2014**, 250, 399–408, DOI:10.1016/j.cej.2014.04.009.
- (42) Bružauskait, I.; Bironait, D.; Bagdonas Eiva Bernotien, E. Scaffolds and Cells for Tissue

Regeneration: Different Scaffold Pore Sizes-Different Cell Effects. DOI:10.1007/s10616-015-9895-4.

- (43) Zhen, W.; Jiang, C.; Feng, B.; Xiaojang, S.; Jianxi, L.; Li, L.; Chen, L.; Rong, D. Role of the Porous Structure of the Bioceramic Scaffolds in Bone Tissue Engineering. *Nat. Preced.* **2010** DOI:10.1038/npre.2010.4148.1.
- (44) Bigi, A.; Boanini, E.; Capuccini, C.; Fini, M.; Mihailescu, I. N.; Ristoscu, C.; Sima, F.; Torricelli, P. Biofunctional Alendronate-Hydroxyapatite Thin Films Deposited by Matrix Assisted Pulsed Laser Evaporation. *Biomaterials* **2009**, *30* (31), 6168–6177, DOI:10.1016/j.biomaterials.2009.07.066.
- (45) Giacomini, D.; Torricelli, P.; Gentilomi, G. A.; Boanini, E.; Gazzano, M.; Bonvicini, F.; Benetti, E.; Soldati, R.; Martelli, G.; Rubini, K.; Bigi, A. Monocyclic  $\beta$ -Lactams Loaded on Hydroxyapatite: New Biomaterials with Enhanced Antibacterial Activity against Resistant Strains. *Sci. Rep.* **2017**, *7* (1), 1–12, DOI:10.1038/s41598-017-02943-2.
- (46) Ishino, T.; Yajin, K.; Takeno, S.; Furukido, K.; Hirakawa, K. Establishment of Osteoblast Culture from Human Ethmoidal Sinus. *Auris Nasus Larynx* **2003**, *30* (1), 45–51, DOI:10.1016/S0385-8146(02)00098-6.
- (47) Busch, E.; Hohenester, E.; Timpl, R.; Paulsson, M.; Maurer, P. Calcium Affinity, Cooperativity, and Domain Interactions of Extracellular EF-Hands Present in BM-40. *J. Biol. Chem.* **2000**, *275* (33), 25508–25515, DOI:10.1074/jbc.M001770200.
- (48) Varoni, E.; Canciani, E.; Palazzo, B.; Varasano, V.; Chevallier, P.; Petrizzi, L.; Dellavia, C.; Mantovani, D.; Rimondini, L. Effect of Poly-L-Lysine Coating on Titanium Osseointegration: From Characterization to in Vivo Studies. *J. Oral Implantol.* **2015**, *41* (6), 626–631, DOI:10.1563/AAID-JOI-D-13-00036.
- (49) E.F. Burguera, H.K. Hockin, L. S. Injectable Calcium Phosphate Cement: Effects of Powder-to-Liquid Ratio and Needle Size. *J. Biomed. Mater. Res. Part B Appl. Biomater.* **2009**, *84* (2), 493–502, DOI:10.1002/jbm.b.30896.Injectable.